GenDR: Lightning Generative Detail Restorator

Yan Wang Shijie Zhao[†] Kai Chen Kexin Zhang Junlin Li Li Zhang ByteDance

Project Page: https://icandle.github.io/gendr_page



Figure 1. Example low-quality input and restoration results from the GenDR † (left) and performance comparison among diffusion-based SR methods (right), both of which demonstrate the advanced performance of the proposed GenDR. (Zoom-in for best view.)

Abstract

Recent research applying text-to-image (T2I) diffusion models to real-world super-resolution (SR) has achieved remarkable success. However, fundamental misalignments between T2I and SR targets result in a dilemma between inference speed and detail fidelity. Specifically, T2I tasks prioritize multi-step inversion to synthesize coherent outputs aligned with textual prompts and shrink the latent space to reduce generating complexity. Contrariwise, SR tasks preserve most information from low-resolution input while solely restoring high-frequency details, thus necessitating sufficient latent space and fewer inference steps. To bridge the gap, we present a one-step diffusion model for generative detail restoration, GenDR , distilled from a tailored diffusion model with larger latent space. In detail, we train a new SD2.1-VAE16 (0.9B) via representation alignment to expand latent space without enlarging the model size. Regarding step-distillation, we propose consistent score identity distillation (CiD) that incorporates SR task-specific loss into score distillation to leverage more SR priors and align the training target. Furthermore, we extend CiD with adversarial learning and representation alignment (CiDA) to enhance perceptual quality and accelerate training. We also polish the pipeline to achieve a more efficient inference. Experimental results demonstrate that GenDR achieves state-of-the-art performance in both quantitative metrics and visual fidelity.

1. Introduction

Image super-resolution (SR) is a classical low-level problem to recover a high-resolution (HR) image from the low-resolution (LR) version [11, 21]. Its core aim is to repair missing high-frequency information from complex or unknown degradation in real-world scenarios with the help of learned priors. To reconstruct more realistically, the existing methods [19, 40] introduce generative adversarial network (GAN) to reproduce the details and have revealed advanced performance. Recently, modernized texto-image (T2I) models, *e.g.*, *Stable Diffusion* (SD) [12, 32] and *PixArt* [6], have demonstrated their ability to synthesize high-resolution images with photographic quality, offering a new paradigm to replenish details.

To assign an image SR objective to these T2I-oriented

[†]Corresponding author.

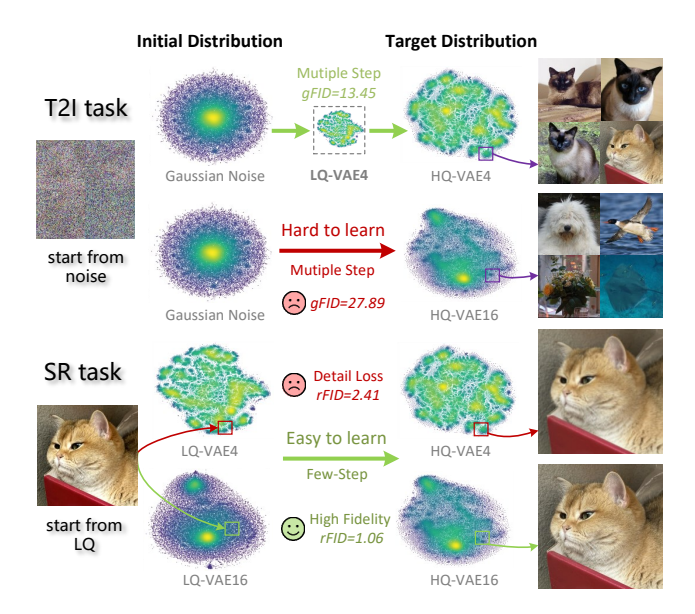


Figure 2. **Motivation**: divergent task objectives make dilemma. T2I task (generation > reconstruction) bridges the huge gap between initial distribution (noise) to target, thus preferring multisteps (better refinement) and narrow latent space (less difficulty) to make results reasonable. SR task (reconstruction > generation) restores only details from adjacent distribution (LQ), needing fewer steps and high-dimensional space. We visualize the latent distribution on ImageNet-val [10] with t-SNE.

diffusion models, current methods [23, 38, 47, 54] leverage additional control modules such as controlnet and encoder to guide a T2I model generating HR image from the noise. Although these methods exhibit superior restoration quality compared to GAN-based methods, two disturbing problems persist that restrict the practical usage of diffusion-based SR: slow inference speed and inferior detail fidelity. To address these issues, OSEDiff [46] employs variational score distillation (VSD) [43] through low-rank adaption (LoRA) [15] to directly distill a one-step SR model from T2I model, which significantly improves throughputs but weakens generation quality. DreamClear [2] employs two controlnets and MLLM-generated prompt to guide PixArt- α [6] generating more faithful results. However, existing methods are caught in the dilemma that improving detail fidelity brings computational overhead (larger base model/additional assistant module), leading to inefficiency while accelerating inference results in unacceptable performance drop since they neglect critical underlying.

As shown in Fig. 2, we identify divergent task objectives between T2I requiring more inference steps and low-dimensional latent space and SR requiring fewer inference steps and high-dimensional latent space as the main contributors to the above problems. This finding is based on the following divergency:

• Divergent generating difficulty: T2I models start from a

sampled Gaussian noise to generate both low-frequency content and high-frequency details aligned with textual prompts. Nevertheless, for SR, the low-frequency structural and semantic components are well-defined in LR, inducing primarily demands on detail restoring. Consequently, SR-tailored diffusion models can theoretically use fewer inference steps to achieve optimal results.

• Divergent reconstruction demends: For T2I, expanding latent space inherently increases model complexity and training difficulty, leading most frameworks to adopt a 4-channel VAE to balance synthesis quality and computational efficiency. Although this trade-off optimizes performance for T2I, it becomes a barrier for reconstruction tasks like SR. VAE4s stumble to preserve intricate details within compressed latent representation, resulting in irreversible detail loss and structural distortion [9, 12].

To address these limitations holistically, this work provides a systematic solution, namely GenDR, for real-world super-resolution (SR), particularly targeting faithful and intricate Generative Detail Restoration. To build this model, we introduce several innovations:

Tailored Base Model. Since SR tasks demand larger latent space, we construct GenDR with a 16-channel base model. However, existing models (*e.g.*, SD3.5 and FLUX) are overqualified for generating details and prohibitively large to exacerbate the dilemma between quality and speed. To address these concerns, based on SD2.1 and an open-source VAE16, we construct an SD2.1-VAE16 as a suitable base model for diffusion-based restoration tasks.

Advanced Step Distillation. To minimize the inference process to one step, we perform step distillation for GenDR. Unlike existing methods [34, 46] that directly employ score distillation from T2I, we integrate task-specific consistent priors from SR into score identity distillation (SiD) [63], proposing Consistent score identity Distillation (CiD), which mitigates adverse effects caused by inconsistencies in the training distribution and over-reliance on imperfect score functions. Furthermore, we introduce CiDA which incorporates CiD with representation Alignment and Adversarial learning to accelerate training and restore high-diversity details, avoiding the "fakeness" of AI-generated image. In practice, we apply low-rank adaption (LoRA) and model-sharing strategies to implement the CiDA training scheme more efficiently.

Simplified Pipeline. We construct a simplified diffusion pipeline comprised solely of VAE and UNet. We remove the scheduler and conditioning modules and use fixed textual embeddings to enable efficient deployment.

Overall, GenDR gains remarkable improvement over existing models in objective quality/efficiency metrics (Tabs. 2 and 3), subjective visual comparison (Fig. 6), and human evaluation (Fig. 7).



Figure 3. 1024²px and 512²px samples produced by SD2.1-VAE16. (Zoom-in for best view.)

Table 1. Comparison of varied T2I methods [6, 31, 32, 34] across GenEval↑ [13] and CLIP↑ [29] on 30K prompts from COCO 2014 [22]. The best and running-up results are **bolded** and underlined.

Model	#Params	GenEval	CLIP
DALL:E	12B	0.23	-
PixArt- α	0.6B	0.48	0.316
SD1.5	0.9B	0.43	0.322
SD2.1	0.9B	0.50	0.30
SD-Turbo	0.9B	-	0.335
SDXL	2.6B	0.55	0.343
SD2.1-VAE16	0.9B	0.48	0.323

2. Related Work

Generative Prior for SR. Existing generative prior-based SR methods can be broadly categorized into GAN prior-based and diffusion prior-based paradigms. GAN-based SR models [39, 40, 59] exploit adversarial training to synthesize visually pleasuring details at the cost of occasional instability during optimization. As a milestone, RealESR-GAN [40] introduced a high-order degradation datapipe to synthesize LR-HR training pairs. Recently, diffusion-based models [2, 23, 38, 46, 47, 50, 56, 58] finetune base model (e.g., UNet and DiT) or train an extra conditioning model (e.g., Encoder and ControlNet) to guide iteratively generation that aligns to the low-quality input. For instance, Diff-BIR [23] introduced a preclear module and IRControlNet to balance fidelity and detail generation. FaithDiff [7] finetuned an auxiliary encoder for SDXL [32].

Step Distillation. To reduce inference cost, massive researchs [24, 28, 33, 34, 43, 52, 63] have focused on distilling multiple-step diffusion processes into few-step frameworks. As a pioneering work, DreamFusion [28] introduced score distillation sampling (SDS) to transfer knowledge from diffusion to arbitrary generators, which paves the way for step distillation. ProlificDreamer [43] and Diffinstruct [25] utilized variational score distillation to enhance generation diversity and stability through probabilistic refinement. SiD [63] further ameliorated the score distillation with identity transformation for stable training.

3. Preliminaries

GAN can produce realistic synthesis by enforcing an adversarial updating between discriminator and generator. Given the generator \mathcal{G} and discriminator \mathcal{D} , GAN cyclically optimizes them with varied adversarial losses:

$$\mathcal{L}^{\mathcal{D}} = \mathbb{E}_{\mathbf{x}_h, \mathbf{x}_g = \mathcal{G}(\mathbf{x}_l)} \left[\ln(1 - \mathcal{D}(\mathbf{x}_g)) + \ln \mathcal{D}(\mathbf{x}_h) \right],$$

$$\mathcal{L}^{\mathcal{G}} = \mathbb{E}_{\mathbf{x}_o} \ln \mathcal{D}(\mathbf{x}_g),$$
(1)

where \mathbf{x}_g , \mathbf{x}_h and \mathbf{x}_l are SR images, high-quality, and low-quality images for SR tasks.

Diffusion model decouples the image synthesis to forward and reverse processes in latent space to stabilize the training and generated quality. For forward diffusion processing, the Gaussian noise $\epsilon \sim \mathcal{N}(0,\mathbf{I})$ is added with the time t-related variance $\beta_t \in (0,1)$ to obtain the immediate latent $\mathbf{z}: \mathbf{z}_t = \bar{\alpha}_t \mathbf{z} + \bar{\beta}_t \epsilon$, where $\alpha_t = 1 - \beta_t$ and $\bar{\alpha}_t = \operatorname{sqrt}(\prod_{s=1}^t \alpha_s)$. During the reverse process, the diffusion model predicts the noise $\hat{\epsilon}$, thus obtaining the initial latent $\hat{\mathbf{z}}_0 = (\mathbf{z}_t - \bar{\beta}_t \hat{\epsilon})/\bar{\alpha}_t$. For SR tasks, a better-starting node, *i.e.*, the LR image \mathbf{z}_l [46], can enable an efficient and simplified reverse function to calculate restored latent \mathbf{z}_a :

$$\mathbf{z}_g = \frac{\mathbf{z}_l - \bar{\beta}_{t_s} \epsilon_{\theta}(\mathbf{z}_l; t_s)}{\bar{\alpha}_{t_s}}, \tag{2}$$

where ϵ_{θ} represents the noise-predicting network.

4. Methodology

4.1. SD2.1-VAE16: 16 channels VAE matters!

To tailor a base model with a larger latent space for the SR task, we develop the UNet from SD2.1 in the latent space of 16-channel VAE². To speed up training, we conduct full-parameter optimization using the REPA strategy [55]. Given input image \mathbf{x}_h , intermediate latent \mathbf{z}_t , encoded output $\mathbf{h}_t = f_{\theta}(\mathbf{z}_t)$, REPA aligns projected results \mathbf{h}_t with the representation $\mathbf{h}_{\mathcal{E}} = \mathcal{E}(\mathbf{x}_h)$ obtained by pre-trained encoder \mathcal{E} , e.g. DINOv2 [27]:

$$\mathcal{L}^{(\text{repa})} = -\mathbb{E}_{\mathbf{x}_h, t} \left[\frac{1}{N} \sum_{n=1}^{N} \sin\left(\mathbf{h}_{\mathcal{E}}[n], h(\mathbf{h}_t[n])\right) \right]. \quad (3)$$

In practice, we insert the multilayer perceptron (MLP) as h after the first downsampling block in UNet. Fig. 3 shows

¹huggingface: stabilityai/stable-diffusion-2-1

²huggingface: ostris/vae-kl-f8-d16

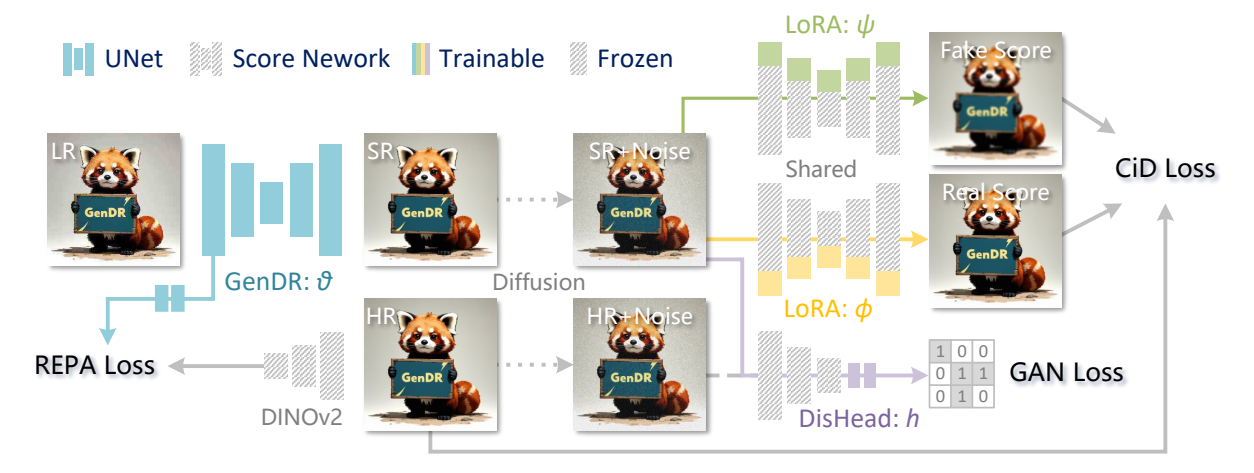


Figure 4. Illustration of the proposed CiDA training scheme for GenDR. GenDR and base score network are initialized with SD2.1-VAE16. The real/fake score network is implemented by LoRA. LR latent is fed into GenDR to restore SR-latent and representation for REPA loss Eq. (3). After diffusion forward pass, noised SR and HR latent are used to calculate CiD loss Eq. (9) and GAN loss Eq. (10).

the visitual results where the proposed SD2.1-VAE16 exhibits impressive generative capability. In Tab. 1, we evaluate the new SD2.1-VAE16 with commonly-used metrics and benchmark datasets, where the SD2.1-VAE16 retains similar performance as the original SD2.1.

To further improve the model's comprehension of image quality attributes, *i.e.*, quality-assessment terminologies like *compressed* and *blurred*, we refine the base model following the DreamClear [2].

4.2. CiD: Consistent Score identity Distillation

The existing score distillation methods [28, 43, 63] are based on the insight: If generator \mathcal{G}_{θ} produces outputs \mathbb{P}_{g} approximating to real data distribution \mathbb{P}_{r} , the score model ψ trained by \mathbb{P}_{g} should converge to pretrained model ϕ trained by \mathbb{P}_{r} .

Score distillation. Given the fixed real score model ϕ and updated fake score model ψ , the restoration network \mathcal{G}_{θ} , generated latent $\mathbf{z}_g = \mathcal{G}_{\theta}(\mathbf{z}_l)$, sampled timestep t, and noise ϵ , the VSD [43] is to cyclingly update θ and ψ by:

$$\nabla_{\theta} \mathcal{L}_{\theta}^{(\text{vsd})} = \mathbb{E}_{t,\epsilon,c,\mathbf{z}_{t} = \bar{\alpha}_{t}\mathbf{z}_{g} + \bar{\beta}_{t}\epsilon} \\ \left[\omega(t) (\epsilon_{\phi}(\mathbf{z}_{t};t,c) - \epsilon_{\psi}(\mathbf{z}_{t};t,c)) \frac{\partial \mathbf{z}_{g}}{\partial \theta} \right], \quad (4)$$

$$\mathcal{L}_{\psi} = \mathbb{E}_{t,\epsilon,c,\mathbf{z}_{t}} \left[||\epsilon_{\psi}(\mathbf{z}_{t};t,c) - \epsilon||^{2} \right],$$

where $\omega(t)$ is a time-aware weighting function. $\epsilon_{\phi,\psi}$ represents scores (noise) predicted by real/fake score networks. Score identity distillation. While VSD provides a tractable framework, it neglects the gradient of the fake score network and is difficult to ensure f_{ψ} achieving convergences, leading to unstable training and susceptibility to local optima due to inadequate convergence guarantees. Following

SiD [63], we leverage score identity transformation to preestimate an ideal value $\epsilon_{\psi}(\mathbf{z}_t;t,c) = -\bar{\beta}_t \nabla_{\mathbf{z}_t} \log p_{\theta}(\mathbf{z}_t)$ for f_{ψ} , incidentally reducing the dependence on f_{ψ} :

$$\mathcal{L}_{\theta}^{(1)} = \mathbb{E}_{t,\epsilon,c,\mathbf{z}_{t} = \bar{\alpha}_{t}\mathbf{z}_{g} + \bar{\beta}_{t}\epsilon} \left[||\epsilon_{\phi}(\mathbf{z}_{t};t,c) - \epsilon_{\psi}(\mathbf{z}_{t};t,c)||^{2} \right] \xrightarrow{\text{SiD}} \mathcal{L}_{\theta}^{(2)} = \mathbb{E}_{t,\epsilon,c,\mathbf{z}_{t}} \left[\omega(t) \langle \epsilon_{\phi}(\mathbf{z}_{t};t,c) - \epsilon_{\psi}(\mathbf{z}_{t};t,c), \epsilon_{\phi}(\mathbf{z}_{t};t,c) - \epsilon \rangle \right].$$
(5)

Consistent score identity distillation. For the SR task, directly applying Eqs. (4) and (5) poses difficulties since T2I (aligning text embedding) and SR (aligning image embedding) have distinct targets and varying training distributions, leading to quality and content inconsistency. Consequently, existing methods [46, 48] employ regression loss (L1, MSE) to ensure consistency between generated latent \mathbf{z}_q and HR target \mathbf{z}_h :

$$\mathcal{L}_{\theta}^{(\text{mse})} = \mathbb{E}_{t,c} \left[||\mathbf{z}_g - \mathbf{z}_h||^2 \right]. \tag{6}$$

To address the issue, we optimize the "fixed" real score network ϕ with z_h to align its output distribution with the target high-fidelity image manifold, which ensures the real score network generates reliable priors for distillation. Following [46, 62], we regulate Eqs. (4) and (5) in latent space and introduce classifier-free guidance (CFG) [14] with quality-related prompts to enhance guidance quality. Overall, the primary CiD can be formulated as follows:

$$\mathcal{L}_{\psi} = \mathbb{E}_{t,\epsilon,c,\mathbf{z}_{t} = \bar{\alpha}_{t}\mathbf{z}_{g} + \bar{\beta}_{t}\epsilon} \left[||f_{\psi}(\mathbf{z}_{t};t,c) - \mathbf{z}_{g}||^{2} \right],$$

$$\mathcal{L}_{\phi} = \mathbb{E}_{t,\epsilon,c,z_{t} = \bar{\alpha}_{t}\mathbf{z}_{h} + \bar{\beta}_{t}\epsilon} \left[||f_{\phi}(\mathbf{z}_{t};t,c) - \mathbf{z}_{h}||^{2} \right],$$

$$\tilde{\mathcal{L}}_{\theta}^{(2)} = \mathbb{E}_{t,\epsilon,c,\mathbf{z}_{t}} \left[\omega(t) \langle f_{\phi,\kappa}(\mathbf{z}_{t};t,c) - f_{\psi,\kappa}(\mathbf{z}_{t};t,c), f_{\phi,\kappa}(\mathbf{z}_{t};t,c) - \mathbf{z}_{g} \rangle \right],$$

$$f_{\kappa}(\mathbf{z}_{t};t,c) = f(\mathbf{z}_{t};t,\varnothing) + \kappa \cdot \left[f(\mathbf{z}_{t};t,c) - f(\mathbf{z}_{t};t,\varnothing) \right],$$
(7)

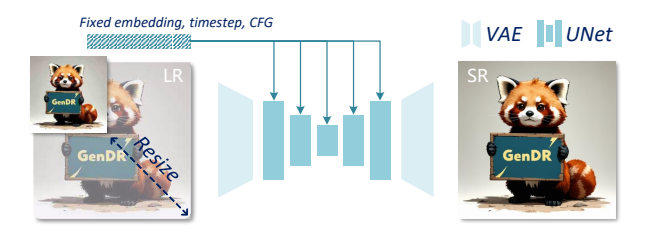


Figure 5. Illustration of proposed GenDR pipeline.

where $f_{\phi,\psi}$ denotes scores (latent) predicted by real/fake score networks. \varnothing represents empty prompt embedding.

Similar to VSD and SiD, the above step distillation framework is data-free and relies on generated results \mathbf{z}_g , which introduce instability due to \mathbf{z}_g 's fluctuating quality and content. To mitigate this, we leverage the optimal latent for θ in Eq. (6) to replace \mathbf{z}_g with \mathbf{z}_h as an identity transformation.

$$\mathcal{L}_{\theta}^{(3)} = \mathbb{E}_{t,\epsilon,c,\mathbf{z}_t} \left[\omega(t) \langle f_{\phi,\kappa}(\mathbf{z}_t;t,c) - f_{\psi,\kappa}(\mathbf{z}_t;t,c), f_{\phi,\kappa}(\mathbf{z}_t;t,c) - \mathbf{z}_h \rangle \right].$$
(8)

Overall, to circumvent the inability to compute $\nabla_{\theta} \psi$, we follow [16, 63] to combine $\mathcal{L}_{\theta}^{(1)}$ and $\mathcal{L}_{\theta}^{(3)}$ through empirical weighting ξ to ensure unbiased optimization:

$$\mathcal{L}_{\theta}^{(\text{cid})} = \mathcal{L}_{\theta}^{(3)} - \xi \mathcal{L}_{\theta}^{(1)}. \tag{9}$$

4.3. CiDA: CiD with Adversary and Alignment

Following DMD2 [51] and REPA [55], we further develop the CiD (Eq. (9)) with adversarial learning and representation alignment. Based on Eq. (1), we examine the generated latent \mathbf{z}_g with pre-trained unet ϕ and extra discriminative heads h:

$$\mathcal{L}_{\theta}^{(\text{adv})} = \frac{1}{H'W'} \sum_{i=1}^{H'} \sum_{j=1}^{W'} \ln h(f_{\phi}(\mathbf{z}_g))[i, j]$$
 (10)

where $H' \times W'$ denotes the spatial dimensions of the discriminator's output feature map.

We also reintroduce representation alignment in Eq. (3) as an effective regularization term. Combined with the CiD objective in Eq. (9) and adversarial loss in Eq. (10), the final target loss integrates:

$$\mathcal{L}_{\theta}^{(\text{cida})} = \lambda_1 \mathcal{L}_{\theta}^{(\text{cid})} + \lambda_2 \mathcal{L}_{\theta}^{(\text{adv})} + \lambda_3 \mathcal{L}_{\theta}^{(\text{repa})}, \tag{11}$$

where $\lambda_{1/2/3}$ are weighting coefficients balancing the contributions of distillation, adversarial, and alignment terms. **Implemetation with LoRA**. CiDA consists of one trainable generator and two trainable score networks, which cost huge GPU memory and computation resources for parameter updating across three UNet. To alleviate this burden, we utilize the low-rank adaptation (LoRA) [15] for fake/real

score networks to reduce the optimizable parameters. In addition, we share the base model for score networks and the feature extractor of the discriminator to further reduce the memory footprint on stowing local models. In Fig. 4, we illustrate the detailed implementation of the proposed CiDA framework. In supplementary material, we present more details for the CiDA training framework.

4.4. GenDR: Simplified Diffusion Pipeline

To enable efficient inference without relying on complex preclear models or conditioning models, we design GenDR using a simplified architecture comprising only a UNet and VAE. Since GenDR executes a one-step calculation, we eliminate the scheduler by empirically assigning $\bar{\alpha}_t = \bar{\beta}_t = 0.5$ across all timesteps t. Additionally, we discard the text encoder and tokenizer, replacing them with several fixed-prompt embeddings stored locally to reduce computational overhead and ensure deterministic generation. Fig. 5 shows the extremely laconic pipeline of GenDR.

5. Experiments

5.1. Experimental Setup

Training details. For SD2.1-VAE16, we train it on selected high-quality images [32, 44]. The training resolution is 512×512 and 1024×1024 which aligns to SD2.1-base and SDXL. We use ZeRO2-Offload [30] and gradient accumulation (steps=8) to extend the batch size to 2048 on 8 NVIDIA A100 GPUs. The fixed learning rate $1e^{-5}$, and default AdamW is adopted to optimize UNet during 100k iterations.

For GenDR, we initialize \mathcal{G}_{θ} and $f_{\phi,\psi}$ with SD2.1-VAE16-512px and conduct full parameter training for \mathcal{G}_{θ} on the LSDIR [20], FFHQ [17], and above-selected images. As to $f_{\phi,\psi}$, we set LoRA rank and alpha as 64 and 128, respectively. Referring to previous setups [23, 46, 47], we randomly crop 512×512 image patches to generate LR-HR pairs through a mixed pipeline of RealESRGAN [40] and APISR [36]. During 50k iteration training, networks are optimized via AdamW optimizers with batchsize 1024 and learning rate $1e^{-5}$ on 8 NVIDIA A100-80G. We set start-timestep $t_s = 500$ for GenDR, and randomly sample timesteps $t \in \{20, ..., 979\}$ for CiDA score networks $f_{\phi,\psi}$. The loss coefficients $\lambda_{1,2,3}$ are 10 (first 10k)/1, 0.01, and 0.1, respectively. Specifically, we use $\omega(t) =$ $C/sg[||\mathbf{z}_h - f_{\phi,\kappa}(\mathbf{z}_t;t,c)||]$ as the time-related function to modulate CiDA loss.

Testing details. Following recent work [41, 56, 57], we evaluate the proposed GenDR with the synthetic dataset ImageNet-Test [10] and several real-world test sets, RealSR [4], RealSet80 [57], and RealLR200 [47]. The ImageNet-Test contains 3000 images under multiple complicated degradations. RealSR has 100 HR-LR image pairs



Figure 6. Visual comparison of GenDR with other methods for ×4 task on RealSet80 dataset. (Zoom-in for best view.)

token by Nikon and Canon cameras. The RealSet80 and RealLR200 contain 80 and 200 low-resolution images without ground truth. In the test phase, we use official codes and settings to examine the compared models for fairness. For GenDR, the positive/negative prompts are fixed to provide a general discription³.

Evaluation metrics and compared methods. We leverage seven commonly used metrics to evaluate image quality, including full-reference metrics (FR-IQA): PSNR, SSIM [42], LPIPS [60], and TOPIQ [5], and noreference metrics (NR-IQA): PI [3], NIQE [26], LIQE [61], MANIQA [49], CLIPIQA [37], MUSIQ [18], ARNIQA [1], Q-Align (Quality) [45], and DepictQA [53]. We also conduct user and MLLM preference studies to obtain a comprehensive evaluation of image quality.

5.2. Comparison with State-of-the-Arts

Quantitative comparison. To comprehensively evaluate the performance of GenDR, we compare it with numerous state-of-the-art methods, including GAN-based models: RealESRAN [40] and RealHATGAN [8], multiple-step diffusion models: StableSR [38], DiffBIR [23], SeeSR [47], and DreamClear [2], one-step diffusion models: SinSR [41], OSEDiff [46], and InvSR [56]. Inclusively, our GenDR obtains superior restoration quality across all three benchmark datasets. As shown in Tab. 3, GenDR surpasses all existing one-step models by a large margin and can compete with multiple-step diffusion models. Specifically, GenDR achieves the highest LIQE, MUSIQ, and Q-Align on all benchmarks. In Tab. 3, we extend the comparison on RealLR200 [47] benchmark.

Moreover, we add total parameters and inference time in Tab. 2, where the GenDR is the fastest and second smallest model. Compared to recent DreamClear, the GenDR gains about $89.5\times$ acceleration and only uses half of the parameters.

^{3&}quot;realism photo, best quality, realistic detailed, clean, high-resolution, best quality, smooth plain area, high-fidelity, clear edge, clean details without messy patterns, high-resolution, no noise, high-fidelity, 4K, 8K, perfect without deformations, photo taken in the style of Canon EOS—style raw"

Table 2. Quantitative comparison (average Parameters, Inference time, and IQA metrics) on both synthetic and real-world benchmarks. The sampling step number is marked in the format of "Method name-Steps" for diffusion-based methods. The best results for all methods are highlighted in **bold** and <u>underlined</u>, while the best *one-step* diffusion methods are reported in *italic*.

	Methods	Base Model				Met	trics			
	Methods	#Params↓	PSNR (dB)↑	SSIM↑	LPIPS↓	NIQE↓	LIQE↑	CLIPIQA↑	MUSIQ↑	Q-Align↑
<i>t</i>	RealESRGAN	GAN-CNN	26.62	0.7523	0.2303	4.4909	3.8414	0.5090	64.81	3.4230
	RealHATGAN	GAN-Trans	27.15	0.7690	0.2044	4.7834	3.5717	0.4594	63.43	3.3244
	StableSR-50	SD 2.1-base	26.00	0.7317	0.2327	4.9378	3.6187	0.5768	64.54	3.4378
Tes	DiffBIR-50	SD 2.1-base	25.45	0.6651	0.2876	4.9289	4.6378	0.7486	73.04	4.3228
'et-	SeeSR-50	SD 2-base	25.73	0.7072	0.2467	4.3530	4.5384	0.6981	72.25	4.2412
ImageNet-Test	DreamClear-50	PixArt- α	24.76	0.6672	0.2463	5.3787	4.4298	0.7646	70.08	4.0919
ma	SinSR-1	LDM	<u>26.98</u>	0.7308	0.2288	5.2506	3.9410	0.6607	67.70	3.8090
I	OSEDiff-1	SD 2.1-base	24.82	0.7017	0.2431	4.2786	4.5609	0.6778	71.74	4.0674
	InvSR-1	SD Turbo	23.81	0.6777	0.2547	4.3935	4.5601	0.7114	72.38	3.9867
	GenDR ⁵ -1	SD 2.1-VAE16	24.14	0.6878	0.2652	4.1336	4.8096	0.7395	<i>74.68</i>	4.3612
	RealESRGAN	16.70M	25.85	0.7734	0.2729	4.6788	3.3372	0.4901	59.69	3.9185
	RealHATGAN	20.77M	<u>26.22</u>	0.7894	0.2409	5.1189	2.8875	0.4336	58.41	3.8353
	StableSR-50	1410M	24.52	0.6733	0.3658	3.4665	3.5612	0.6897	66.87	3.9862
~	DiffBIR-50	1717M	26.28	0.7251	0.3187	5.8009	3.3588	0.6743	64.28	3.9182
ISF	SeeSR-50	2524M	26.19	0.7555	0.2809	4.5366	3.7728	0.6826	66.31	3.9862
RealSR	DreamClear-50	2212M	24.14	0.6963	0.3155	3.9661	3.5452	0.6730	63.74	3.9705
_	SinSR-1	119M	25.99	0.7072	0.4022	6.2412	3.0034	0.6670	59.22	3.8800
	OSEDiff-1	1775M	24.57	0.7202	0.3036	4.3408	3.9634	0.6829	67.30	4.0664
	InvSR-1	1289M	24.50	0.7262	0.2872	4.2218	<u>4.0346</u>	<u>0.6919</u>	<u>67.47</u>	<u>4.2085</u>
	GenDR ⁵ -1	933M	23.18	0.7135	0.2859	4.1588	4.1906	0.7014	68.36	4.2388
	Methods	Time↓	PI↓	ARNIQA↑	DepictQA↑	NIQE↓	LIQE↑	CLIPIQA↑	MUSIQ↑	Q-Align↑
	RealESRGAN	36ms	3.8843	0.6538	-	4.1517	3.7392	0.6190	64.49	4.1696
RealSet80	RealHATGAN	116ms	4.1817	0.6578	-	4.4705	3.4927	0.5502	63.21	4.1077
	StableSR-50	3731ms	3.0314	0.6776	33.78%	3.3999	3.8516	0.7399	67.58	4.0870
	DiffBIR-50	6213ms	3.9544	0.6802	33.15%	5.1389	4.0472	<u>0.7404</u>	68.72	<u>4.3206</u>
	SeeSR-50	6359ms	3.7454	0.7170	51.61%	4.3749	4.2797	0.7124	69.74	4.3056
ealt	DreamClear-50	6892ms*	<u>3.4157</u>	0.6738	52.93%	<u>3.7257</u>	3.9628	0.7242	67.22	4.1206
Re	SinSR-1	120ms	4.2697	0.6638	30.82%	5.6103	3.5957	0.6634	63.79	4.0954
	OSEDiff-1	103ms	3.6894	0.6883	<u>66.49%</u>	3.9763	4.1298	0.7037	69.19	4.3057
	InvSR-1	115ms	3.4524	0.7172	53.14%	4.0266	<u>4.2906</u>	0.7271	69.79	4.3014
	GenDR [*] -1	77ms	3.5518	0.7321	<i>78.14%</i>	3.9750	4.5248	0.7424	71.57	4.4525

^{*:} inference time calculated under using 3 A100 GPU to run an image.

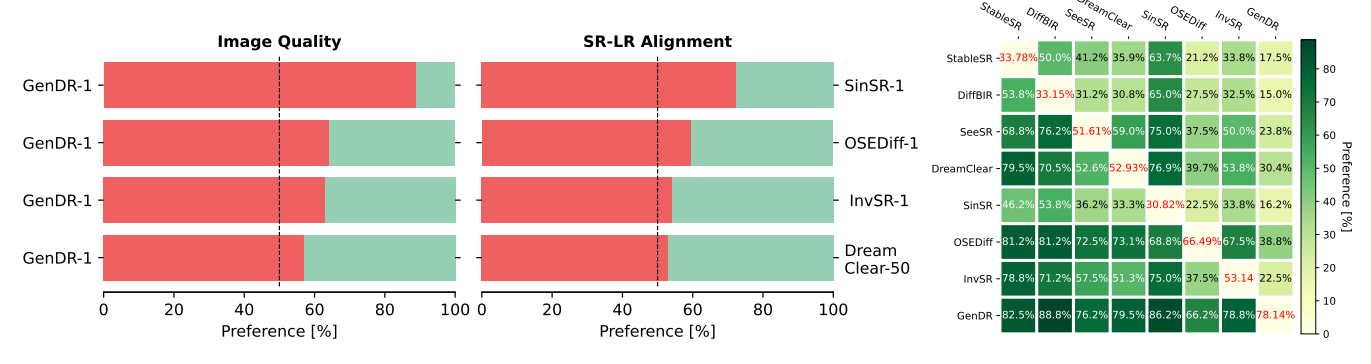


Figure 7. User preference study on image quality and SR-LR alignment.

Figure 8. DepictQA preference.

Qualitative comparision. Fig. 6 exhibits the visual comparison for GenDR with other approaches. Generally, GenDR presents the best quality in terms of blurry removal and detail recovery. For *Image 9* from RealSet80 [57], GenDR is the only model to restore the entire chrysanthe-

mum and correctly split foreground and background. As to *Image 50*, GenDR recovers a more vivid bird with clearer eyes and feathers from the degraded input. The visual results demonstrate the splendid recovery performance of the proposed GenDR.

Table 3. Extented quantitative comparison on RealLR200.

Methods	Metrics↑							
	LIQE	MANIQA	CLIPIQA	MUSIQ	Q-Align			
RealESRGAN	3.4837	0.3688	0.5408	62.96	3.8895			
SinSR	3.5061	0.4435	0.5996	63.77	3.9187			
OSEDiff	4.0496	0.4298	0.6666	69.03	4.2534			
InvSR	4.0779	0.4368	0.6830	68.90	4.2125			
GenDR 5	4.4656	0.4882	0.7269	72.36	4.4768			

Table 4. Ablation study on varied distillation loss on RealSet80.

Methods	Strategies	Metrics↑					
	Strategies	LIQE	CLIPIQA	MUSIQ	Q-Align		
OSEDiff	VSD	4.1298	0.7037	69.19	4.3057		
	CiDA	4.3184	0.7230	70.13	4.3858		
GenDR 5	VSD	4.1248	0.6911	68.82	4.3732		
	SiD	4.2528	0.7016	69.33	4.3912		
	CiD	4.4432	<u>0.7150</u>	<u>70.61</u>	4.4278		
	CiDA	4.5248	0.7424	71.57	4.4525		

Table 5. Ablation study on varied inference setting for GenDR.

Prompt	Prompt	Prompt	Time	#Params	#MACs	MUSIQ
	Extract Time	Embed Time	Time	mi didilis		
Null	-	15ms	92ms	1263M	1637G	70.66
DAPE	21ms	15ms	113ms	1775M	2638G	71.74
Qwen2.5	3.09s	16ms	3.18s	8.3B	-	71.08
Fixed	-	15ms	<u>92ms</u>	<u>1263M</u>	<u>1637G</u>	71.57
Fixed	-	-	77ms	933M	1623G	<u>71.57</u>

User studies and MLLM evaluation. For a thorough comparison between diffusion-based SR, We conduct user studies to compare images restored by GenDR against SinSR [41], OSEDiff [46], and DreamClear [2]. Fig. 7 shows that our GenDR convincingly outperforms other diffusion-based models. For further evaluation, in Fig. 8, we use DepictQA [53], an advanced MLLM, to make pairwise comparisons and calculate the average selected rate (in red). The GenDR receives about 78% votes, indicating its better quality than other methods.

5.3. Ablation Study

Effectiveness of CiD and CiDA. To examine the effectiveness of the proposed distillation approach, we use VSD [43], SiD [63], CiD, and CiDA to distill OSED-iff [46]/GenDR. The Tab. 4 shows the quantitative comparisons, where the proposed CiDA yields a 0.08 improvement on Q-Align for both OSEDiff and GenDR. Specific to each loss function, the CiD accounts for 0.05 on Q-Align and adversarial learning contributes the remaining 0.03.

Effectiveness of 16 channel VAE. As exhibited in Tab. 4, compared to GenDR-VSD with 16-channel VAE, OSEDiff-VSD with 4-channel VAE have similar or even higher objective scores. However, they are rather different in subjective comparison, specifically for details preserving and generating. In Fig. 9, we compare the model with 4/16 chan-



Figure 9. Visual comparison between models with VAE4 and VAE16, both of which are distilled by VSD loss.

nel latent in detail. The SD2.1-VAE4 model is smoother and clearer, which is preferred by metrics. In contrast, the SD2.1-VAE16-based model has more faithful details and can maintain the small textures or texts, which wins more selection from users.

Effectiveness of simplified pipeline. For more efficient inference, we replace the text encoding modules and scheduler in GenDR with fixed embeddings. In Tab. 5, we compare the proposed GenDR pipeline with different prompt extractors (DAPE [47], Qwen2.5-7B [35]) and strategies, where our design is the most efficient and maintains a similar IQA score with content-related prompts. We provide more results on prompt selection in supp-material.

6. Conclusion

This work presents GenDR fror real-world SR by tailoring the T2I model in an SR-favored manner, *i.e.*, using high-dimensional latent space to preserve and generate more details and one-step inference to improve efficiency. In detail, we develop an SD2.1-VAE16 providing a better trade-off between reconstruction quality and efficiency. Based on it, we introduce a consistent score identity distillation (CiD) that incorporates SR priors into T2I-oriented step diffusion to promote consistency and stability. Moreover, we improve CiD with adversarial learning and REPA to achieve better realistic details. Overall, GenDR obtains a remarkable quality-efficiency trade-off.

References

- Lorenzo Agnolucci, Leonardo Galteri, Marco Bertini, and Alberto Del Bimbo. Arniqa: Learning distortion manifold for image quality assessment. In WACV, pages 189–198, 2024. 6
- [2] Yuang Ai, Xiaoqiang Zhou, Huaibo Huang, Xiaotian Han, Zhengyu Chen, Quanzeng You, and Hongxia Yang. Dreamclear: High-capacity real-world image restoration with privacy-safe dataset curation. *NeurIPS*, 37:55443–55469, 2025. 2, 3, 4, 6, 8
- [3] Yochai Blau, Roey Mechrez, Radu Timofte, Tomer Michaeli, and Lihi Zelnik-Manor. The 2018 pirm challenge on perceptual image super-resolution. In ECCVW, pages 0–0, 2018.
- [4] Jianrui Cai, Hui Zeng, Hongwei Yong, Zisheng Cao, and Lei Zhang. Toward real-world single image super-resolution: A new benchmark and a new model. In *ICCV*, pages 3086– 3095, 2019. 5
- [5] Chaofeng Chen, Jiadi Mo, Jingwen Hou, Haoning Wu, Liang Liao, Wenxiu Sun, Qiong Yan, and Weisi Lin. Topiq: A top-down approach from semantics to distortions for image quality assessment. *IEEE TIP*, 2024. 6
- [6] Junsong Chen, Jincheng Yu, Chongjian Ge, Lewei Yao, Enze Xie, Yue Wu, Zhongdao Wang, James Kwok, Ping Luo, Huchuan Lu, et al. Pixart-α: Fast training of diffusion transformer for photorealistic text-to-image synthesis. arXiv preprint arXiv:2310.00426, 2023. 1, 2, 3
- [7] Junyang Chen, Jinshan Pan, and Jiangxin Dong. Faithdiff: Unleashing diffusion priors for faithful image superresolution. *arXiv preprint arXiv:2411.18824*, 2024. 3
- [8] Xiangyu Chen, Xintao Wang, Jiantao Zhou, Yu Qiao, and Chao Dong. Activating more pixels in image superresolution transformer. In CVPR, pages 22367–22377, 2023.
- [9] Xiaoliang Dai, Ji Hou, Chih-Yao Ma, Sam Tsai, Jialiang Wang, Rui Wang, Peizhao Zhang, Simon Vandenhende, Xiaofang Wang, Abhimanyu Dubey, et al. Emu: Enhancing image generation models using photogenic needles in a haystack. arXiv preprint arXiv:2309.15807, 2023. 2
- [10] Jia Deng, Wei Dong, Richard Socher, Li-Jia Li, Kai Li, and Li Fei-Fei. Imagenet: A large-scale hierarchical image database. In CVPR, pages 248–255, Miami, USA, 2009. IEEE Computer Society. 2, 5
- [11] Chao Dong, Chen Change Loy, Kaiming He, and Xiaoou Tang. Image super-resolution using deep convolutional networks. *IEEE TPAMI*, 38(2):295–307, 2016.
- [12] Patrick Esser, Sumith Kulal, Andreas Blattmann, Rahim Entezari, Jonas Müller, Harry Saini, Yam Levi, Dominik Lorenz, Axel Sauer, Frederic Boesel, et al. Scaling rectified flow transformers for high-resolution image synthesis. In *ICML*, 2024. 1, 2
- [13] Dhruba Ghosh, Hannaneh Hajishirzi, and Ludwig Schmidt. Geneval: An object-focused framework for evaluating text-to-image alignment. *NeurIPS*, 36:52132–52152, 2023. 3
- [14] Jonathan Ho and Tim Salimans. Classifier-free diffusion guidance. *arXiv preprint arXiv:2207.12598*, 2022. 4

- [15] Edward J Hu, Yelong Shen, Phillip Wallis, Zeyuan Allen-Zhu, Yuanzhi Li, Shean Wang, Lu Wang, Weizhu Chen, et al. Lora: Low-rank adaptation of large language models. *ICLR*, 1(2):3, 2022. 2, 5
- [16] Zemin Huang, Zhengyang Geng, Weijian Luo, and Guojun Qi. Flow generator matching. arXiv preprint arXiv:2410.19310, 2024. 5
- [17] Tero Karras, Samuli Laine, and Timo Aila. A style-based generator architecture for generative adversarial networks. In CVPR, pages 4401–4410, 2019. 5
- [18] Junjie Ke, Qifei Wang, Yilin Wang, Peyman Milanfar, and Feng Yang. Musiq: Multi-scale image quality transformer. In CVPR, pages 5148–5157, 2021. 6
- [19] Christian Ledig, Lucas Theis, Ferenc Huszár, Jose Caballero, Andrew Cunningham, Alejandro Acosta, Andrew Aitken, Alykhan Tejani, Johannes Totz, Zehan Wang, et al. Photorealistic single image super-resolution using a generative adversarial network. In CVPR, pages 4681–4690, 2017. 1
- [20] Yawei Li, Kai Zhang, Jingyun Liang, Jiezhang Cao, Ce Liu, Rui Gong, Yulun Zhang, Hao Tang, Yun Liu, Denis Demandolx, et al. Lsdir: A large scale dataset for image restoration. In CVPRW, pages 1775–1787, 2023. 5
- [21] Bee Lim, Sanghyun Son, Heewon Kim, Seungjun Nah, and Kyoung Mu Lee. Enhanced deep residual networks for single image super-resolution. In CVPRW, pages 1132–1140, 2017.
- [22] Tsung-Yi Lin, Michael Maire, Serge Belongie, James Hays, Pietro Perona, Deva Ramanan, Piotr Dollár, and C Lawrence Zitnick. Microsoft coco: Common objects in context. In ECCV, pages 740–755. Springer, 2014. 3
- [23] Xinqi Lin, Jingwen He, Ziyan Chen, Zhaoyang Lyu, Bo Dai, Fanghua Yu, Yu Qiao, Wanli Ouyang, and Chao Dong. Diffbir: Toward blind image restoration with generative diffusion prior. In *ECCV*, pages 430–448. Springer, 2024. 2, 3, 5, 6
- [24] Simian Luo, Yiqin Tan, Longbo Huang, Jian Li, and Hang Zhao. Latent consistency models: Synthesizing highresolution images with few-step inference. arXiv preprint arXiv:2310.04378, 2023. 3
- [25] Weijian Luo, Tianyang Hu, Shifeng Zhang, Jiacheng Sun, Zhenguo Li, and Zhihua Zhang. Diff-instruct: A universal approach for transferring knowledge from pre-trained diffusion models. *NeurIPS*, 36:76525–76546, 2023. 3
- [26] Anish Mittal, Rajiv Soundararajan, and Alan C Bovik. Making a "completely blind" image quality analyzer. *IEEE Sign. Process. Letters*, 20(3):209–212, 2012. 6
- [27] Maxime Oquab, Timothée Darcet, Théo Moutakanni, Huy Vo, Marc Szafraniec, Vasil Khalidov, Pierre Fernandez, Daniel Haziza, Francisco Massa, Alaaeldin El-Nouby, et al. Dinov2: Learning robust visual features without supervision. arXiv preprint arXiv:2304.07193, 2023. 3
- [28] Ben Poole, Ajay Jain, Jonathan T Barron, and Ben Mildenhall. Dreamfusion: Text-to-3d using 2d diffusion. *arXiv* preprint arXiv:2209.14988, 2022. 3, 4
- [29] Alec Radford, Jong Wook Kim, Chris Hallacy, Aditya Ramesh, Gabriel Goh, Sandhini Agarwal, Girish Sastry, Amanda Askell, Pamela Mishkin, Jack Clark, et al. Learning transferable visual models from natural language supervision. In *ICML*, pages 8748–8763. PmLR, 2021. 3

- [30] Samyam Rajbhandari, Jeff Rasley, Olatunji Ruwase, and Yuxiong He. Zero: Memory optimizations toward training trillion parameter models. In SC20: International Conference for High Performance Computing, Networking, Storage and Analysis, pages 1–16. IEEE, 2020. 5
- [31] Aditya Ramesh, Mikhail Pavlov, Gabriel Goh, Scott Gray, Chelsea Voss, Alec Radford, Mark Chen, and Ilya Sutskever. Zero-shot text-to-image generation. In *ICLR*, pages 8821–8831. Pmlr, 2021. 3
- [32] Robin Rombach, Andreas Blattmann, Dominik Lorenz, Patrick Esser, and Björn Ommer. High-resolution image synthesis with latent diffusion models. In CVPR, pages 10684– 10695, 2022. 1, 3, 5
- [33] Axel Sauer, Frederic Boesel, Tim Dockhorn, Andreas Blattmann, Patrick Esser, and Robin Rombach. Fast high-resolution image synthesis with latent adversarial diffusion distillation. In *SIGGRAPH Asia*, pages 1–11, 2024.
- [34] Axel Sauer, Dominik Lorenz, Andreas Blattmann, and Robin Rombach. Adversarial diffusion distillation. In ECCV, pages 87–103. Springer, 2024. 2, 3
- [35] Qwen Team. Qwen2.5: A party of foundation models, 2024.
- [36] Boyang Wang, Fengyu Yang, Xihang Yu, Chao Zhang, and Hanbin Zhao. Apisr: anime production inspired real-world anime super-resolution. In CVPR, pages 25574–25584, 2024. 5
- [37] Jianyi Wang, Kelvin CK Chan, and Chen Change Loy. Exploring clip for assessing the look and feel of images. In AAAI, pages 2555–2563, 2023. 6
- [38] Jianyi Wang, Zongsheng Yue, Shangchen Zhou, Kelvin CK Chan, and Chen Change Loy. Exploiting diffusion prior for real-world image super-resolution. *IJCV*, 132(12):5929– 5949, 2024. 2, 3, 6
- [39] Xintao Wang, Ke Yu, Shixiang Wu, Jinjin Gu, Yihao Liu, Chao Dong, Yu Qiao, and Chen Change Loy. Esrgan: Enhanced super-resolution generative adversarial networks. In ECCVW, pages 0–0, 2018. 3
- [40] Xintao Wang, Liangbin Xie, Chao Dong, and Ying Shan. Real-esrgan: Training real-world blind super-resolution with pure synthetic data. In CVPR, pages 1905–1914, 2021. 1, 3, 5, 6
- [41] Yufei Wang, Wenhan Yang, Xinyuan Chen, Yaohui Wang, Lanqing Guo, Lap-Pui Chau, Ziwei Liu, Yu Qiao, Alex C Kot, and Bihan Wen. Sinsr: diffusion-based image superresolution in a single step. In CVPR, pages 25796–25805, 2024. 5, 6, 8
- [42] Zhou Wang, Alan C. Bovik, Hamid R. Sheikh, and Eero P. Simoncelli. Image quality assessment: from error visibility to structural similarity. *IEEE TIP*, 13(4):600–612, 2004. 6
- [43] Zhengyi Wang, Cheng Lu, Yikai Wang, Fan Bao, Chongxuan Li, Hang Su, and Jun Zhu. Prolificdreamer: High-fidelity and diverse text-to-3d generation with variational score distillation. *NeurIPS*, 36, 2024. 2, 3, 4, 8
- [44] Zijie J Wang, Evan Montoya, David Munechika, Haoyang Yang, Benjamin Hoover, and Duen Horng Chau. Diffusiondb: A large-scale prompt gallery dataset for text-to-image generative models. *arXiv preprint arXiv:2210.14896*, 2022. 5

- [45] Haoning Wu, Zicheng Zhang, Weixia Zhang, Chaofeng Chen, Liang Liao, Chunyi Li, Yixuan Gao, Annan Wang, Erli Zhang, Wenxiu Sun, et al. Q-align: teaching lmms for visual scoring via discrete text-defined levels. In *ICML*, pages 54015–54029, 2024. 6
- [46] Rongyuan Wu, Lingchen Sun, Zhiyuan Ma, and Lei Zhang. One-step effective diffusion network for real-world image super-resolution. *NeurIPS*, 2024. 2, 3, 4, 5, 6, 8
- [47] Rongyuan Wu, Tao Yang, Lingchen Sun, Zhengqiang Zhang, Shuai Li, and Lei Zhang. Seesr: Towards semantics-aware real-world image super-resolution. In CVPR, pages 25456– 25467, 2024. 2, 3, 5, 6, 8
- [48] Rui Xie, Chen Zhao, Kai Zhang, Zhenyu Zhang, Jun Zhou, Jian Yang, and Ying Tai. Addsr: Accelerating diffusionbased blind super-resolution with adversarial diffusion distillation. arXiv preprint arXiv:2404.01717, 2024. 4
- [49] Sidi Yang, Tianhe Wu, Shuwei Shi, Shanshan Lao, Yuan Gong, Mingdeng Cao, Jiahao Wang, and Yujiu Yang. Maniqa: Multi-dimension attention network for no-reference image quality assessment. In CVPR, pages 1191–1200, 2022. 6
- [50] Tao Yang, Rongyuan Wu, Peiran Ren, Xuansong Xie, and Lei Zhang. Pixel-aware stable diffusion for realistic image super-resolution and personalized stylization. In ECCV, pages 74–91. Springer, 2024. 3
- [51] Tianwei Yin, Michaël Gharbi, Taesung Park, Richard Zhang, Eli Shechtman, Fredo Durand, and William T Freeman. Improved distribution matching distillation for fast image synthesis. *arXiv preprint arXiv:2405.14867*, 2024. 5
- [52] Tianwei Yin, Michaël Gharbi, Richard Zhang, Eli Shechtman, Fredo Durand, William T Freeman, and Taesung Park. One-step diffusion with distribution matching distillation. In CVPR, pages 6613–6623, 2024. 3
- [53] Zhiyuan You, Zheyuan Li, Jinjin Gu, Zhenfei Yin, Tianfan Xue, and Chao Dong. Depicting beyond scores: Advancing image quality assessment through multi-modal language models. In ECCV, pages 259–276. Springer, 2024. 6, 8
- [54] Fanghua Yu, Jinjin Gu, Zheyuan Li, Jinfan Hu, Xiangtao Kong, Xintao Wang, Jingwen He, Yu Qiao, and Chao Dong. Scaling up to excellence: Practicing model scaling for photorealistic image restoration in the wild. In CVPR, pages 25669–25680, 2024. 2
- [55] Sihyun Yu, Sangkyung Kwak, Huiwon Jang, Jongheon Jeong, Jonathan Huang, Jinwoo Shin, and Saining Xie. Representation alignment for generation: Training diffusion transformers is easier than you think. arXiv preprint arXiv:2410.06940, 2024. 3, 5
- [56] Zongsheng Yue, Kang Liao, and Chen Change Loy. Arbitrary-steps image super-resolution via diffusion inversion. arXiv preprint arXiv:2412.09013, 2024. 3, 5, 6
- [57] Zongsheng Yue, Jianyi Wang, and Chen Change Loy. Resshift: Efficient diffusion model for image superresolution by residual shifting. *NeurIPS*, 36, 2024. 5, 7
- [58] Aiping Zhang, Zongsheng Yue, Renjing Pei, Wenqi Ren, and Xiaochun Cao. Degradation-guided one-step image super-resolution with diffusion priors. *arXiv preprint* arXiv:2409.17058, 2024. 3

- [59] Kai Zhang, Jingyun Liang, Luc Van Gool, and Radu Timofte. Designing a practical degradation model for deep blind image super-resolution. In *ICCV*, pages 4791–4800, 2021. 3
- [60] Richard Zhang, Phillip Isola, Alexei A Efros, Eli Shechtman, and Oliver Wang. The unreasonable effectiveness of deep features as a perceptual metric. In CVPR, pages 586–595, 2018. 6
- [61] Weixia Zhang, Guangtao Zhai, Ying Wei, Xiaokang Yang, and Kede Ma. Blind image quality assessment via vision-language correspondence: A multitask learning perspective. In *CVPR*, pages 14071–14081, 2023. 6
- [62] Mingyuan Zhou, Zhendong Wang, Huangjie Zheng, and Hai Huang. Long and short guidance in score identity distillation for one-step text-to-image generation. *arXiv preprint arXiv:2406.01561*, 2024. 4
- [63] Mingyuan Zhou, Huangjie Zheng, Zhendong Wang, Mingzhang Yin, and Hai Huang. Score identity distillation: Exponentially fast distillation of pretrained diffusion models for one-step generation. In *ICML*, 2024. 2, 3, 4, 5, 8